Asian Journal of Chemistry; Vol. 32, No. 9 (2020), 2347-2355

ASIAN JOURNAL OF CHEMISTRY

https://doi.org/10.14233/ajchem.2020.22769

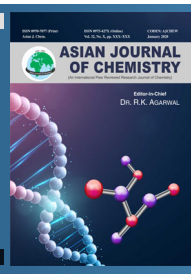

Structural, Optical, Electrical and Photocatalytic Degradation Properties of Cadmium Sulfide Nanopaticles by Sol Gel Methodd

M. SANKAR[1], M. JOTHIBAS[1,*], A. MUTHUVEL[1] and B. ARUN KUMAR[2]

[1]PG and Research Department of Physics, T.B.M.L. College (Affiliated to Bharathidasan University, Tiruchirappalli), Porayar-609307, India
[2]Department of Physics, Sir Issac Newton Arts & Science College, Pappakovil, Nagapattinam-611102, India

*Corresponding author: E-mail: jothibas1980@gmail.com

Received: 11 April 2020; *Accepted*: 26 June 2020; *Published online*: 20 August 2020; AJC-20037

Cadmium sulfide (CdS) nanoparticles were synthesized *via* inexpensive sol gel method at different sintering temperature (350, 400 and 450 °C). The synthesized CdS nanoparticles have been characterized by X-ray diffraction, UV-visible spectroscopy, photoluminescence spectroscopy, scanning electron microscopy, high resolution transmission electron microscopy and Fourier transform infrared spectroscopy. The XRD pattern confirmed the formation of hexagonal Wurtzite structure for all the sintering temperatures. The crystallite size, microstrain and dislocation density have been evaluated using XRD data. SEM and HR-TEM analysis showed morphological transformation with better crystallite and spherical shaped CdS nanoparticles were observed. EDS is also performed to confirm the elemental composition of CdS nanoparticles. FT-IR analysis identified the absorption peaks of the Cd-S extension with moisture content. The UV-visible spectra showed absorption peak in the range of 223-257 nm and optical band gap decrease with increase of sintering temperatures. In addition the synthesized CdS nanoparticles were effectively used to degrade methyl orange dye under sunlight irradiation. The CdS nanoparticles were the potential candidate for optoelectronic applications.

Keywords: CdS, Sol-gel, Crystallite size, Photocatalytic, I-V, Methylene orange dye.

INTRODUCTION

Generally, nanoparticles can be defined as a particle ranging in size from 1 to 100 nm, meaning that it acts as a link between the macroscopic and the microscopic world. Heavy metal ions and additional inorganic and organic elements in metal-oxide nanoparticles are exceptional in their form, morphology, functional groups and electronic properties. Nanoparticles have established much interest due to their unique properties and their probable applications in different fields such as light emitters, transistors, optoelectronics and optical devices [1-4]. Semiconductor nanoparticles have characteristic optical, surface morphological and electronic properties and have been widely study for many relevant applications. In parti-cularly, electrical properties of semiconducting nanoparticles as a occupation of particles size, shape, capping agent, optical band gap, *etc*. holds a significant importance in the research of nanoscience and technology. Influence of different external parameters like precursor concentration temperature, types of doping on the electrical properties of semiconductors is widely investigated by many researchers for the past years [5]. Nanostructures sulfides and selenides (CdS, CdSe, ZnSe and ZnS) have been extensively investigated to determine the relationship between structure, size and optical properties. These sulfides are used for a variety of applications such as, photo detector, light emitting diode, solar cells, photovoltaic, sensors, photoluminescence and transistors due to size reduction and cost effect. Among various semiconductor materials cadmium sulfide (CdS) is an II-VI, n-type semiconductor having direct bandgap energy of 2.4 eV at room temperature. Cadmium sulfide (CdS) nanoparticles have attracted a great attention for their potential application in variety fields such as field emitters, gas sensors, varistors and solar cells. Recently, there has been growing interest in photocatalytic applications of CdS. The confinement effect is observed for CdS nanoparticles when sizes are equal to or less than 50 Å [6]. The CdS exits in three types of crystalline structure namely hexagonal Wurtzite, zinc blend and high pressure rack salt phase. The total Wurtzite system is a thermo-

dynamically established segment below regular conditions (such as room temperature and atmospheric pressure). The divergence in essential energy between these two phases is small. It was assumed that the phase permanence between the zinc composite and the Wurtzite structures of CdS depends on. Among these, hexagonal phase is the mostly stable and has been found compare to other two phases. Nanoparticles of CdS having large surface to volume ratio and imperfect surface making it a potential candidate for various applications, such as field of transistor, laser screen materials, photovoltaic cell, biosensor and photocatalytic activity [7]. The synthesis of CdS nanoparticles is important for large-scale engineering applications in the field of microelectronics, photosynthesis and catalysis. Numbers of synthesis methods have previously been employed by different researches to prepare CdS nanoparticles such as solid state reaction, chemical precipitation, wet chemical methods, microemulation, electrochemical methods and sol-gel method [8-13]. The sol-gel method has comparative advantages such as simplicity, ease handling and low-cost processing of the various methods above the synthesis of CdS nanoparticles. In particular, this method is suitable for the development of huge excellent crystals with high surface area and different morphologies by varying the precursor concentration, reaction temperature and time. CdS nanoparticles are made of various cadmium source precursors, cadmium nitrate, cadmium acetate, cadmimum sulfate and cadmium chloride. Hydrogen sulfide gas, sodium sulfide and thiourea are commonly used for the solution based preparation of nanomaterialized CdS. Using semiconductor photocatlytic under ultraviolet or sunlight radiation can eliminate harmful organic contaminants in air and wastewater. CdS has been proposed as a potential candidate in photocatalytic due to their narrow band gap. Kumar and Sharma [14] have studied the effect of temperature on structural, optical and photocatalytci properties of CdS nanoparticles. Khatter and Chauhan [15] the effect of temperature on properties of CdS nanostructures synthesized by solvothermal method. Khan *et al.* [16] reported the solvothermal method used synthesized CdS nanoaprticles degraded the methylene blue dye at 95% for 80 min. In the present work, the synthesis of CdS nanoparticles *via* sol gel method has been reported. The synthesized CdS nanoparticles have been characterized with the help of X-ray diffraction, UV-visible spectroscopy, photoluminescence spectroscopy, scanning electron microscopy; high resolution transmission electron microscopy and Fourier transform infrared spectroscopy. In addition the synthesized CdS nanoparticles were photocatalytic activity and I-V characteristics are studied. The results were discussed in terms of photocatalytic and electrical properties with crystal shape and size.

EXPERIMENTAL

Analytical grades solvents and chemicals *viz*. cadmium acetate, sodium hydroxide, acetone, absolute ethanol and methyl orange dye were purchased from Sigma-Aldrich Chemicals and used as received. Double distilled water was used to prepare the solutions.

Synthesis of CdS nanoparticles: CdS nanoparticles are prepared by sol-gel method. The synthesis was carried out in the aqueous medium. 0.1 M of cadmium acetate dissolved in 50 mL of double distilled water and stirred for 30 min. Then 4 mL of PEG was dissolved into the above solution with constant stirring until the homogenous solution is formed. Then 20 mL of thiourea dissolved in 50 mL of distilled water and added dropwise in to the above solution. The orange precipitate of CdS is formed after the stirring of 6 h. The precipitate was washed several times with distilled water and filtered Whatman No. 1 filter paper. Subsequentially, the precipitated was dried at 100 °C for 24 h. Finally the product was sintering at 350 ºC for 2 h in muffle furnace. The dried powder samples were used further analysis. This experiment was repeated in used for different sintering temperatures in 350, 400 and 450 ºC.

Characterization: The crystalline phase purity of CdS nanoparticles was examined by X-ray diffraction analysis using SHIMADZU 6000 X-ray diffractometer with Cu$K\alpha$ radiation (k = 1.5406 Å) at room temperature. The optical absorption spectra were recorded in the range 200-500 nm utilizing JASCO V-670 spectrophotometer. The photoluminescence behaviour was studied at romm temperature by plorolog 3-HORIBA JOBIN YVON with an excitation wavelength of 325 nm. The morphologies of the particles were affirmed by SEM and HR-TEM (Hitachi S-4500 SEM Machine). FT-IR spectra were recorded with an FT-IR (2000) Perkin Elmer using a KBr plate at room temperature in the 4000-400 cm^{-1} range with a scanning rate of 4 cm^{-1}/min to identify the presence of functional groups of CdS nanoaprticles. The current-voltage (I-V) relationship of the CdS nanoparticles recorded using keithely source meter (model-2450)

Photocatalytic experiment: The photodegradation of methyl orange dye under sunlight irradiation was carried out in the presence of CdS nanoparticles. The stock solution of dye was prepared by dissolving 10 mg of methyl orange dye in 500 mL of water. Before illumination, the suspension of CdS nanoparticles (0.06 g CdS in 100 mL dye solution) in dye was stirred in dark for 60 min, to equilibrate the solution. After equilibration of solution, the suspension was illuminated in indigenous sunlight reactor for 75 min, till the dark orange colour was changed to colourless. The concentration of methyl orange dye in the samples was purposive using UV-vis spectrophotometer. The percentage of methyl orange absorbed on the catalyst surface was calculated from the following equation [17]:

$$\text{Degradation (\%)} = \frac{C_o - C_t}{C_o} \times 100 \quad (1)$$

where C_o represent the initial in absorption and C_t represent the absorption after various time intervals.

RESULTS AND DISCUSSION

The study of CdS nanoparticles was performed using sol gel method at different sintering temperature (350, 400 and 450 ºC). The temperature increases the prepared CdS nanoparticles colour change brown to orange, this types of changes due to primary conform of CdS nanoparticles.

Structural analysis: The crystallite size and phase structure of XRD pattern of CdS nanoparticles synthesized at different sintering temperatures are depicted in Fig. 1. The XRD pattern is revealed from diffraction angle 20° to 80° and all the results compared with JCPDS card No. 65-3414. All the prepared samples polycrystalline nature with hexagonal wurtzite structure. No other diffraction peaks were observed, suggesting the absence of spurious phases in the samples at observable XRD levels. Apparently, the XRD pattern exhibits three dominant broad peaks positioned at 2θ = 26.4, 28.0 and 24.8° with are, respectively assigned to (100), (002) and (101) diffraction peaks of the hexagonal wurtzite phase. Such diffractive pattern is volubly to be referred as the nature of nanosized particles, which also agree with these reported for CdS nanoparticles [18]. According to Jothibas *et al.* [19], the observed peaks indicate that the CdS nanoparticles are the smallest crystal size in nature. Fig. 1 shows the peaks that represent the (002) plane that represent the (002) plane posses highest intensity, compare to other plane (100) and (101) moreover, the intensity of the peaks increased slightly with increase of sintering temperature at 400 ºC. However, the sintering temperature increase at 450 °C, the (002) plane was decreases with increase the intensity of the plane (100) and (101) if can still be observed from the Fig. 1, the sintering temperature of 450 °C is well matched with reported value [20].

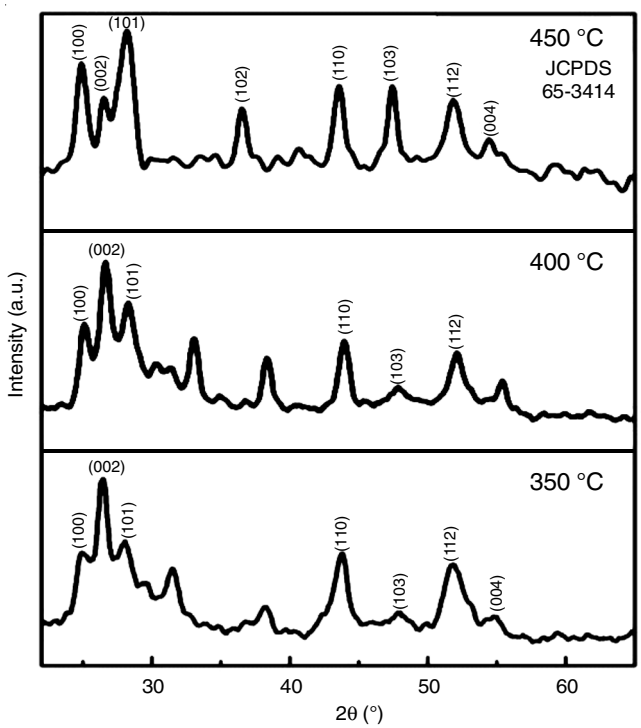

Fig. 1. XRD spectra of CdS nanoparticles at different sintering temperatures

The structural parameters like average crystallite size, microstrain and dislocation density are estimated from XRD data. Debye-Scherrer's formula is used to estimate the structural parameters of CdS nanoparticles [21]:

$$D = \frac{0.09\lambda}{\beta\cos\theta} \quad (2)$$

The dislocation density (δ) and microstrain (ε) are calculated using the following equations:

$$\varepsilon = \frac{\beta\cos\theta}{4} \quad (3)$$

$$\delta = \frac{1}{D^2} \text{ lines/m}^2 \quad (4)$$

where D is the crystallite size, θ is Bragg angle, β is the full width at half maximum (FWHM), k is a shape factor (k = 0.9 in this work), λ is the wavelength of incident X-rays (λ = 0.15406 nm), (hkl) are the Miller indices.

As the sintering temperature increase average crystallite size increased from 7.8 to 9.4 nm, respectively. Table-1 shows the variation in sintering temperatures causes change crystallite size. The average crystallite size increase with increasing sintering temperature up to 450 °C. This may be due to the fact that, in CdS nanoparticles have number of vacancies of oxygen vacancy clusters and local lattice disorders present at the interface, which leads to the decrease in the volume of the unit cell. Low temperature (350 °C) can lead to relaxation in the interface structure, but does not eliminate the local lattice disorder or change the internal structure of the CdS nanoparticles. Sintering temperature (400 °C) is a rapid restart of lattice parameters and the volume of the unit cell is normal and when the grains begin to grow. The increase in crystalline size at higher sintering temperatures (450 °C) demonstrates the growth of large-scale particles during sintering and is attributed to the coordination of small grains by grain boundary diffusion [22]. The value of microstrain decreased from 4.2445 to 3.3939 lines/m^2 and dislocation density also decease with increase of sintering temperatures from 350, 400 and 450 °C leads to better crystallite shown in Table-1. The small crystallite size of the

TABLE-1
STRUCTURAL PARAMETERS OF SYNTHESIZED CdS NANOPARTICLES AT DIFFERENT TEMPERATURES

Samples	FWHW	2θ (°)	Miller indices (hkl)	Dislocation density (δ) × 10^{15} (L/m^2)	Micro strain (ε × 10^{-3})	Crystal size D (nm)	Average crystal size (nm)
350 °C	1.00000	26.6500	(002)	16.86625	4.24355	7.7	7.8
	1.48000	28.2000	(101)	36.98224	6.25978	5.2	
	0.73340	24.0500	(100)	8.89996	3.12804	10.6	
400 °C	0.83640	26.4318	(002)	11.81474	3.55087	9.2	8.2
	1.50000	28.0606	(101)	38.44675	6.33380	5.1	
	0.75000	24.8000	(100)	9.42595	3.19444	10.3	
450 °C	1.07500	28.0875	(101)	19.83733	4.56193	5.1	9.4
	0.70000	24.8750	(100)	7.43162	2.96284	10.3	
	0.80000	26.4667	(002)	10.85069	3.39594	9.2	

synthesized CdS nanoparticles by sol gel method compared to the other methods as shown in Table-2. The present work shows that the acquisition of CdS nanoparticles from a smaller crystal size (9.4 nm) by the sol-gel method can greatly improve activity of photocatalytic.

Morphological analysis: The analysis of SEM microscopy was used to characterize the shape and size of the formed CdS nanopartciles. The SEM image of CdS nanoparticles synthesized with three different sintering temperatures (350, 400 and 450 ºC) are shown in Fig. 2a-c. The morphology of all the samples are spherical shaped and nanosized rings. All phenomena accumulate as the reaction temperature rises, which is

TABLE-2
COMPARISON OF CRYSTALLITE SIZE OF CdS NANOPARTICLES PREPARED FROM DIFFERENT METHODS

Material used	Synthesis method	Crystaillie size (nm)	References
CdS-NPs	Sol gel	9.40	Present work
CdS-NPs	Co-preciptation	15.23	[15]
CdS-NPs	Solvothermal	19.22	[16]
CdS-NPs	Chemical precipitate	10.12	[17]
CdS-NPs	Hydrothermal	32.66	[23]
CdS-NPs	Laser ablation	13.00	[24]
CdS-thin film	Spray pyrolysis	13.00	[25]

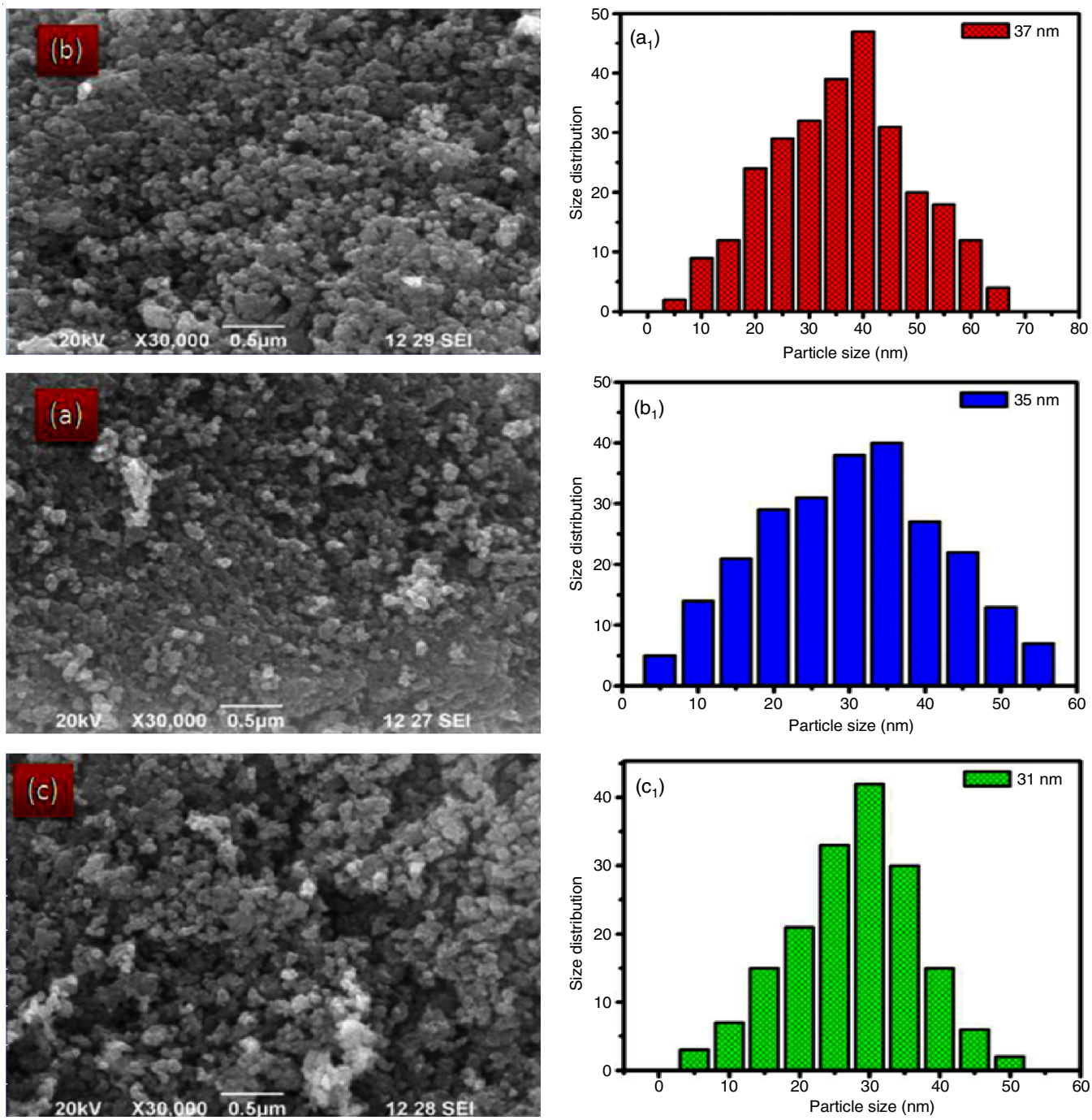

Fig. 2. (a-c) SEM images (a_1-c_1) Histrogram of particles size distrubution of synthesized CdS nanoparticles at different temperatures

due to the development of the uncontrolled parts of the Ostwald uunning [26]. The synthesis of CdS nanoparticles, mainly two reaction mechanisms are involved. Principally, during crystal growth, *in situ* precursor heating, Ostwald follows an important pathway for ripening, in which the surface energy is reduced when large particles are formed by using smaller particles. However, the ripening of nanoparticles is driven by many parameters such as precursor temperature, organism reactivity, thus identifying two-time depositional growth of CdS nanoparticles. When the temperature is raised, the rate of formation of the nuclei is faster than that of the inferior decomposition temperature, which is entirely slow. Moreover, the matrix acts as a response chamber in which the crystal can barely produce to a convinced extent, preventing the cohesion of the nanoparticles. Continuously, polymer chain removal promotes aggregation of particles and aggregation of previously built units When the temperature is raised, the rate of formation of the nuclei is faster than that of the inferior decomposition temperature, which is entirely slow [27]. As the sintering temperture is prolonged to 450 °C, the spin dle-like structure transforms into spherical nanoparticles with lesser agglomeration. A clear morphological change is noticed on varying the 450 °C temperture. Fig. 2(a_1-c_1) shows the histrogram of particle size distribution indicates the mean diameter of CdS nanoparticles as 37, 35 and 31 nm for 350, 400 and 450 °C, respectively. The copostional anaysis using EDS spectrum of CdS nanoparticles (optimized sintering teperature 450 °C) are shown in Fig. 2d. Cd and S peaks are clearly found from EDS analysis. The atomic percentage is 88.72%, 61.27% and wegihy percentage are 15.17, 84.12% corresponding to S and Cd, respectively.

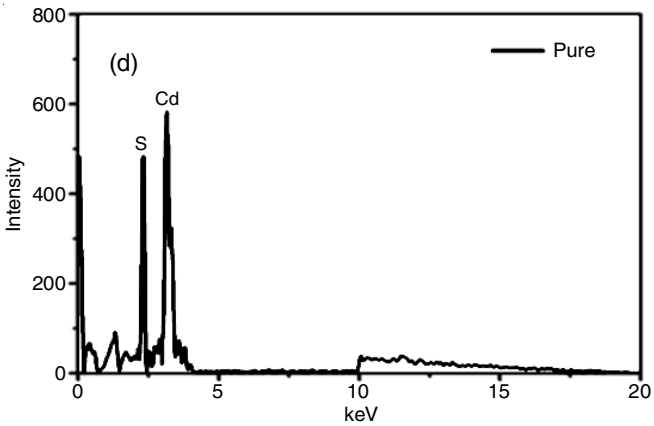

Fig. 2. (d) EDS spectrum of synthesized CdS nanoparticles with sintering temperatures (450 °C)

The crystal structure of synthesized CdS nanoparticles with sintering tempeture (450 °C) was investigated using High resolution transmission electron microscopy. Fig. 3 shows the HR-TEM image of synthesized CdS nanoparticles. The HR-TEM images show the spherical shaped particles (Fig. 3a). The averge particle size 28 nm for synthesizd CdS nanoparticles shows in Fig. 3b. Fig. 3c show the SAED pattern of the synthesized CdS nanoparticles (100), (002) and (101) diffraction peaks of the hexagonal wurtzite phase, which matches with XRD analysis.

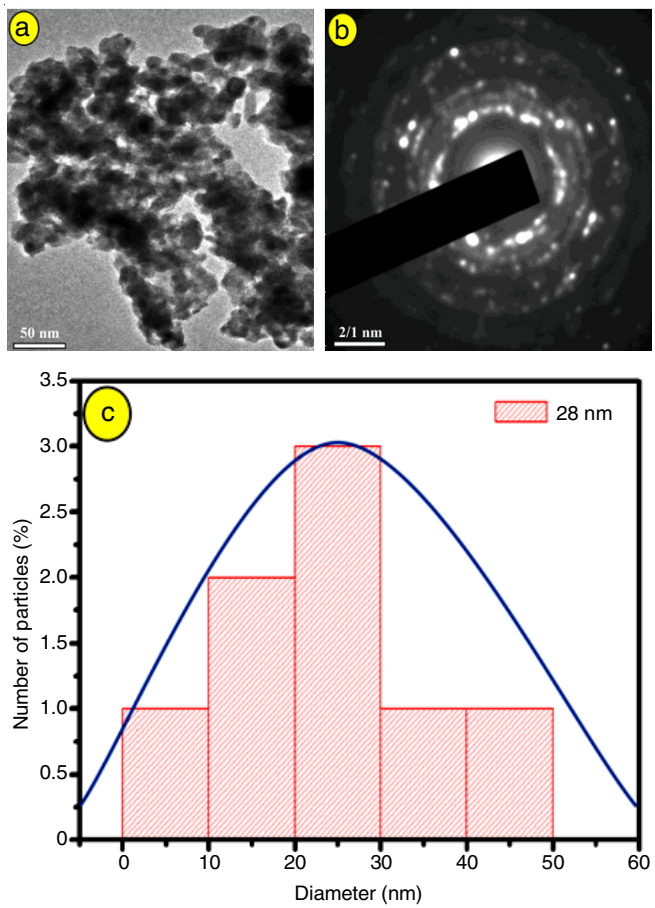

Fig. 3. (a) HR-TEM image (b) SAED pattern (c) particle size of synthesized CdS nanoparticles with sintering temperatures (450 °C)

Functional group analysis: Fourier transform infrared spectroscopy is used to investigate infrared spectral absorption or sample transfer. FT-IR is utilized to examine the composition and quality of CdS nanoparticles prepared with ethylenediamine as solvent nanostructures synthesis at optimized sintering temperature (450 °C) by sol-gel method. Fig. 4 shows the FT-IR spectra of synthesized CdS nanoparticles with sintering temperatures (450 °C). In the FT-IR spectrum of CdS nanoparticles, the strong absorption peaks at 3461cm^{-1} (N-H streteching in amines), 2351 cm^{-1} (O-H strectching in carboxylic acids), 1548 cm^{-1} (N-H bending in amines), 1114 cm^{-1} (C-H bending in aromatic ring), respectively [21]. The strong absorption band in the region from 600 to 700 cm^{-1} is due to the Cd-S stretching vibration. The similar kinds of results obtained for CdS nanoparticles was reported by Ayodhya *et al*. [28].

Optical analysis: One of the main features of the semiconductor is their optical behaviour. CdS nanoparticles synthesized at different sintering temperatures show sharp apsorption spectra in the wavelength range 200-500 nm. The absorption edge observed at 223, 242 and 257 nm for CdS nanoparticles at 350, 400 and 450 °C, respectively (Fig. 5). All the samples exhibited strong absorption peak in the UV-visible region. A red shift in the absorption specrtum was at 450 °C due to aqualitative indication of the crystal size distrubution. The optical band gap of CdS nanoparticles with different sintering temperatures is estimated by Tauc's formula from absorption data according to these equations [17]:

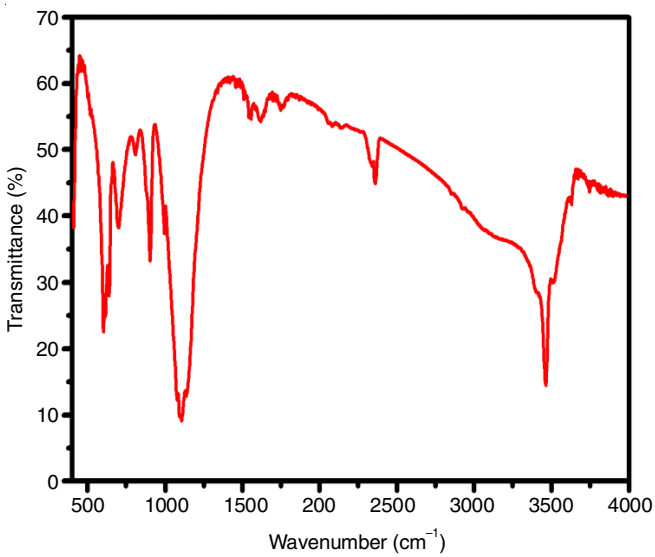

Fig. 4. FT-IR spectra of synthesized CdS nanoparticles with with sintering temperatures (450 °C)

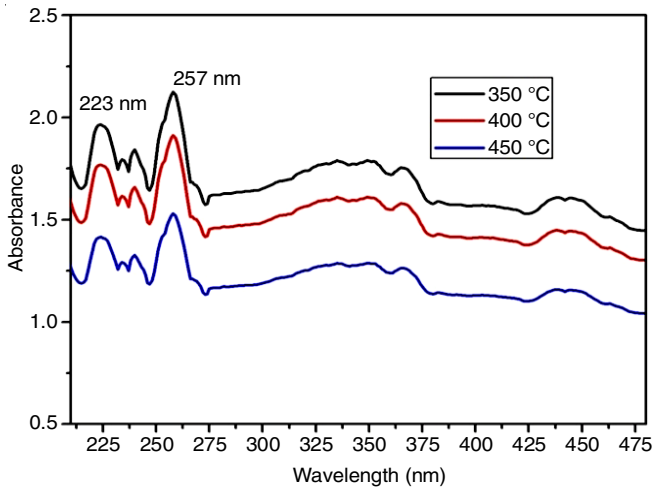

Fig. 5. UV-Visible spectra of synthesized CdS nanoparticles at different sintering temperatures

$$\alpha h\nu = A\,(h\nu - E_g)^{1/2} \quad (5)$$

where α is the optical absorption coefficient, hν is the photon energy, E_g is the direct band gap and A is an energy independent constant, hν and extra plating the linear the linear portion of the absorption edge to find the intercept with energy axis is shown in Fig. 6.

The value of optical band gap of CdS nanoparticles are calculated to be 2.45, 2.39 and 2.35 eV synthesized at 350 °C, 400 °C and 450 °C, respectively. The optical band gap decrease with increase of sintering temperatures. The decrease of optical band gap value for CdS nanoparticles with sintering temperature are in well matched with the crystallite size as extracted from XRD analysis. The decrease of band gap value as compared to bulk CdS (Eg = 2.4 eV) indicates the quantum confinement effect [29]. This band gap energy (Eg = 2.35 eV) is very low compared to the CdS nanoparticles using Co-precipitation method [15]. The present work shows that the acquisition of CdS nanoparticles from small band gap values by the sol-gel method can greatly improve the photocatalytic activity.

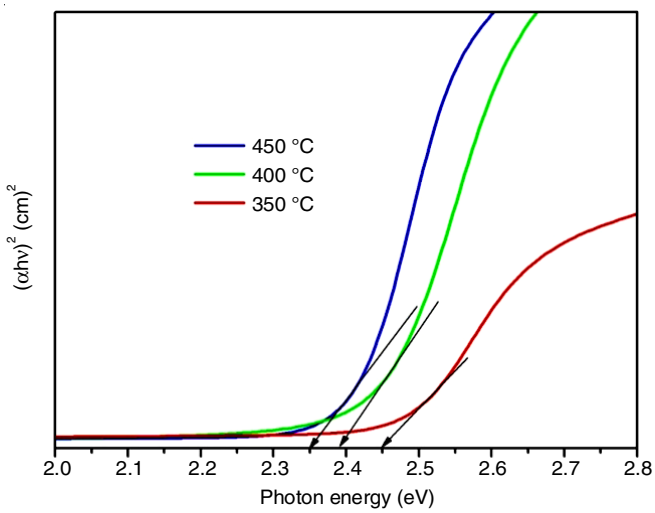

Fig. 6. Plot of $(\alpha h\nu)^2$ *vs.* hν for synthesized CdS nanoparticles at different sintering temperatures

Photoluminescence analysis: Photoluminescence (PL) studies are applicable to obtain an information on the different energy levels available between the valence and conduction bands that are responsible for the radiative recombination. Photoluminescence spectra for the synthesized CdS nanoparticles sintered at different temperatures are shown in Fig. 7. Pure CdS NPs exhibits emission peaks at two sharp shoulder peaks 418, 439 nm and one broad peak 585 nm were observed. The PL emission centered at 418 nm is attributed to excitanic recombination consequent to near band edge (NBE) emission of CdS [30]. The emission in the blue region at about 439 nm is associated with the electronic transition between excitanic levels to interstitial level [31]. The broad peak orange emission observed at 585 nm, this orange emission may be due to the transition between interstitial cadmium donor level and acceptor level located at higher energies with respect to the valence band [16]. Also, sintering temperature increases with decrease of PL emission, it may be due to the structural phase transition.

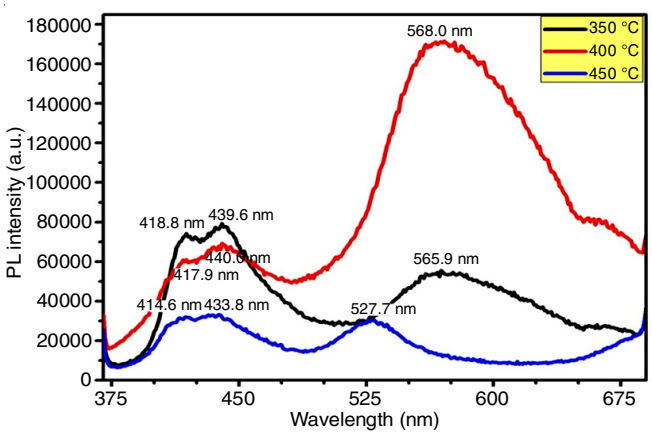

Fig. 7. PL spectra of synthesized CdS nanoparticles at different sintering temperatures

Electrical properties: Room temperature current-voltage characteristic is a measure for CdS nanoparticles synthesized in different sintering temperatures (350, 400 and 450 ºC). All the

peaks are ohmic nature, the current-voltage (I-V) characteristics of the CdS nanoparticles showed a semi-conducting behaviour (Fig. 8). It is because of wide band gap (2.35 eV) and higher work functions. This will result into formation of Schottky barrier having valuable high speed rectifying properties [32]. It is clearly evident from I-V characteristics that value of current get increased across the voltage of -10 to 10 V with increase in temperature. Grain boundaries play the vital role of potential barrier and scattering of charge carriers with these grain boundaries. An increase in average crystallite size with increase of sintering temperatures as discussed in XRD analysis. The optical band gap value of CdS nanoparticles is found to be decreased with increase in sintering temperature, hence, electrical current get increased with sintering temperature [33]. It is observed that the maximum electrical current for CdS nanoparticles synthesized at 450 ºC due to large crystallite size and minimum optical band gap value. From this observation it is clear that the CdS nanoparticles are photo sensitivity and can be used for detection of different wavelength of light based on its I-V characteristics.

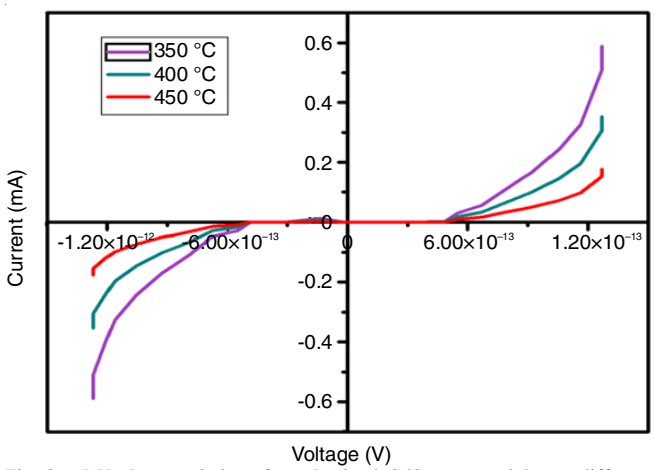

Fig. 8. I-V characteristics of synthesized CdS nanoparticles at different sintering temperatures

Photocatalytic activity: Due to its low cost of methyl orange dye, readily available and high performance in the textile industries an effective fungicide in the aquaculture production and in the paper, leather and pharamaceutical industries [34]. It is greatly toxic to mammalian cells, carcinogogenic and cause skin irritation. Therefore, removal of methyl orange dye from effluent is essential to protect the environmental. The photocatalytic activity of sol gel method used synthesized CdS nanoparticles (450 ºC) was assayed for methyl orange dye under sunlight irradiation. The absorbance spectra of methyl orange dye were recorded (Fig. 9a) at different time intervals in the presence of CdS nanoparticles. The degradation of methyl orange dye was measured at absorbance at 264 and 464 nm, respectively. The calculated degradation effectiveness of methyl orange was 89%, respectively (Table-3). It has been report that the photocatalytic activity can be strong depending on the shape, size of the nanoparticles and generation process and consumption of photogenerated carriers [17]. The photoactive sites on the photocatalyst would be increased by surface area of the crystalline structure, which could enhance the photocatalytic recation electron-hole pairs [35]. Therefore, the results of the experiments performed in this study have clearly declared that CdS nanoparticles potential photocatalytic activities against methyl orange dye.

TABLE-3
EFFECT OF METHYL ORANGE DYE DEGRADATION BY SYNTHESIZED CdS NANOPARTICLES WITH SINTERING TEMPERATURE (450 °C)

Time (min)	Degradation of methyl orange dye (%)
0	0
15	22
30	31
45	45
60	62
75	89

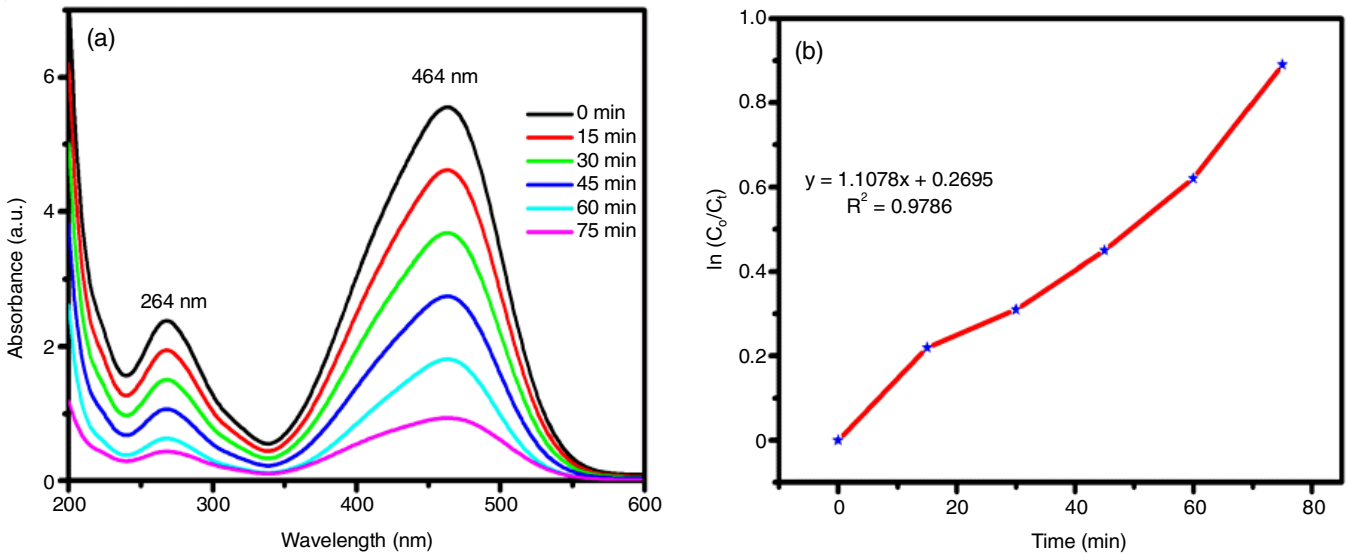

Fig. 9. (a) UV-Vis absorption spectra of methylene orange dye with respect to irradiation time *versus* (b) rate constant (K) and regression (R^2) of synthesized CdS nanoparticles with sintering temperatures (450 °C)

Mechanism for photocatalytic degradation: The CdS nanoparticles are irradiated by sunlight the electron (e^-) in the valence band transfer to the conduction band by absorbing energy leaving behind a hole (h^+) in the valance band. Thus e^-–h^+ pairs are created and these charge carrier go to the surface. The holes corrode the water molecules OH^- ions to form hydroxyl hydroxyl radicals ($^\bullet OH$), the electrons oxidize atmospheric oxygen and form superoxide radicals ($^\bullet O_2^-$). The formation of pores and electrons in the valence band and conduction band plays an important role in the degradation of dye. The reaction mechanism for the photocatalyst is given below:

$$CdS + h\nu \longrightarrow CdS\ (e^- + h^+) \quad (6)$$

$$CdS\ (h^+) + OH^- \longrightarrow OH^\bullet \quad (7)$$

$$CdS\ (e^+) + O_2 \longrightarrow O_2^{\bullet-} \quad (8)$$

$$O_2^{\bullet-} + H^+ \longrightarrow OH^{2\bullet} \quad (9)$$

$$CdS\ (e^-) + H^+ + HO_{2\bullet} \longrightarrow OH^\bullet + OH^- \quad (10)$$

$$O_2^{\bullet-} + HO_{2\bullet} + OH^\bullet\ (or)\ (h^+) +$$

Methyl orange dye degradation product

Colour dye decomposition is mainly recognized for the surface charge, morphology and size property of CdS nanoparticles. Photon-induced molecular reaction occur on the surface of the catalyst in a photocatalytic system. Photon-induced electron pores facilitate redox reactions against the surface of the catalyst and form superoxide ions and hydroxyl free radicals. These created radicals act as powerful photocatalyst to dissolve pollutant chemicals in the wastewater [35].

Kinetic studies: It is understood that the degradation of methyl orange dye by photocatalysts mainly follows pseudo first-order kinetics [17]:

$$\ln\left(\frac{C}{C_o}\right) = kt \quad (11)$$

where, k is the first-order reaction rate constant.

In Fig. 9b shows the C/C_o as a function of reaction time for the degradation of methyl orange dye for CdS nanoparticles. The curve is linear for CdS nanoparticles which signify that the kinetic of the photoatalytic degradation of methyl orange follows pseudo first order reaction rate. The reaction rate constant (k) can be obtained from the slope of the curve. The first order rate constant (k) obtained from Fig. 9b are 0.9786 min^{-1} of methyl orange dye for CdS nanoparticles, respectively, which demonstrate that methyl orange dye for the cadmium sulfide significantly improves the photocatalytic activity. The above results, suggest that the synthesized CdS nanoparticles by sol gel method show better photocatalytic activity on methyl orange dye compare to the hydrothermal method [23].

Conclusion

The II-VI semiconducting CdS nanoparticles are successfully synthesized by sol-gel method at three different sintering temperatures (350, 400 and 450 °C). The influence of different temperature on the different characterization of CdS nanoparticles was investigated. From the results, we conclude that XRD analysis was confirmed the hexagonal wurtzite structure of CdS nanoparticles and the crystallite size can between 7.8-9.4 nm. The SEM photographs the change in surface morphology of CdS nanoparticles with the influence of sintering temperatures and also exhibits spherical shaped grains were observed. The optical band gap changed in the range from 2.45-2.35 eV. The strong UV-vis emission and broad blue-orange emission peaks were observed PL spectra, which confirmed the optical quality of CdS nanoparticles. The synthesized CdS nanoparticles effectively degraded the dye when nearly 89% of the methyle orange dye was decomposed at 75 min of exposure time. All the finding suggests utilization of CdS nanoparticles can be used in electronic devices and optoelectronic application.

CONFLICT OF INTEREST

The authors declare that there is no conflict of interests regarding the publication of this article.

REFERENCES

1. L. Liu, H. Song, L. Fan, F. Wang, R. Qin, B. Dong, H. Zhao, X. Ren, G. Pan, X. Bai and Q. Dai, *Mater. Res. Bull.*, **44**, 1385 (2009); https://doi.org/10.1016/j.materresbull.2008.11.023
2. V. Singh, P.K. Sharma and P. Chauhan, *Mater. Charact.*, **62**, 43 (2011); https://doi.org/10.1016/j.matchar.2010.10.009
3. P. Kumar, *Nanoscale Res. Lett.*, **5**, 1367 (2010); https://doi.org/10.1007/s11671-010-9696-9
4. R. Seoudi, A.A. Shabaka, M. Kamal, E.M. Abdelrazek and W. Eisa, *Physica E*, **45**, 47 (2012); https://doi.org/10.1016/j.physe.2012.07.006
5. H. Das and P. Datta, *Mater. Res. Express*, **6**, 045023 (2019); https://doi.org/10.1088/2053-1591/aafaaa
6. M. Pal, N.R. Mathews, P. Santiago and X. Mathew, *J. Nanopart. Res.*, **14**, 916 (2012); https://doi.org/10.1007/s11051-012-0916-3
7. N.V. Hullavarad, S.S. Hullavarad and P.C. Karulkar, *J. Nanosci. Nanotechnol.*, **8**, 3272 (2008); https://doi.org/10.1166/jnn.2008.145
8. J. Yu, Y. Yu, P. Zhou, W. Xiao and B. Cheng, *Appl. Catal. B*, **156-157**, 184 (2014); https://doi.org/10.1016/j.apcatb.2014.03.013
9. R. Gupta, *J. Crit. Rev.*, **6**, 1 (2019); https://doi.org/10.22159/jcr.2019v6i5.34073
10. L. Qi, J. Ma, H. Cheng and Z. Zhao, *Colloids Surf. A Physicochem. Eng. Asp.*, **111**, 195 (1996); https://doi.org/10.1016/0927-7757(96)03545-5
11. R.K. Sonker, B.C. Yadav, V. Gupta and M. Tomar, *Mater. Chem. Phys.*, **239**, 121975 (2020); https://doi.org/10.1016/j.matchemphys.2019.121975
12. A.E. Mahmoud, H.S. Wasly and M.A. Doheim, *J. Eng. Sci. (Assiut Univ.)*, **42**, 1430 (2014).
13. M.S. Abd El-Sadek, H.S. Wasly and K.M. Batoo, *Appl. Phys., A Mater. Sci. Process.*, **125**, 283 (2019); https://doi.org/10.1007/s00339-019-2576-y
14. S. Kumar and J.K. Sharma, *Mater. Sci. Pol.*, **34**, 368 (2016); https://doi.org/10.1515/msp-2016-0033
15. J. Khatter and R.P. Chauhan, *J. Mater. Sci. Mater. Electron.*, **31**, 2676 (2020); https://doi.org/10.1007/s10854-019-02807-7
16. Z.R. Khan, M. Zulfequar and M.S. Khan, *J. Mater. Sci.*, **46**, 5412 (2011); https://doi.org/10.1007/s10853-011-5481-0
17. A. Muthuvel, M. Jothibas, C. Manoharan and S.J. Jayakumar, *Res. Chem. Intermed.*, **46**, 2705 (2020); https://doi.org/10.1007/s11164-020-04115-w

18. R.G. Solanki, P. Rajaram and P.K. Bajpai, *Indian J. Phys.*, **92**, 595 (2018); https://doi.org/10.1007/s12648-017-1134-8
19. M. Jothibas, C. Manoharan, S.J. Jeyakumar, P. Praveen and I.J. Panneerdoss, *J. Mater. Sci. Mater. Electron.*, **27**, 5851 (2016); https://doi.org/10.1007/s10854-016-4502-9
20. S. Suganya, M. Jothibas and S.J. Jeyakumar, *J. Mater. Sci. Mater. Electron.*, **30**, 7916 (2019); https://doi.org/10.1007/s10854-019-01113-6
21. R. Elilarassi, S. Maheshwari and G. Chandrasekaran, *Optoelectron. Adv. Mater. Rapid Commun.*, **4**, 309 (2010).
22. R.M. German, *Crit. Rev. Solid State Mater. Sci.*, **35**, 263 (2010); https://doi.org/10.1080/10408436.2010.525197
23. R. Rajendran, K. Varadharajan and V. Jayaraman, *Colloids Surf. A Physicochem. Eng. Asp.*, **580**, 123688 (2019); https://doi.org/10.1016/j.colsurfa.2019.123688
24. A.N. Abd, R.A. Ismail and N.F. Habubi, *J. Mater. Sci. Mater. Electron.*, **26**, 9853 (2015); https://doi.org/10.1007/s10854-015-3660-5
25. A.A. Yadav and E.U. Masumdar, *J. Alloys Compd.*, **509**, 5394 (2011); https://doi.org/10.1016/j.jallcom.2011.02.061
26. K. Manzoor, S.R. Vadera, N. Kumar and T.R.N. Kutty, *Solid State Commun.*, **129**, 469 (2004); https://doi.org/10.1016/j.ssc.2003.11.012
27. H.C. Warad, S.C. Ghosh, B. Hemtanon, C. Thanachayanont and J. Dutta, *Sci. Technol. Adv. Mater.*, **6**, 296 (2005); https://doi.org/10.1016/j.stam.2005.03.006
28. D. Ayodhya, M. Venkatesham, A. Santoshi kumari, G. Bhagavanth Reddy and G. Veerabhadram, *Int. J. Ind. Chem.*, **6**, 261 (2015); https://doi.org/10.1007/s40090-015-0047-7
29. R.R. Prabhu and M.A. Khadar, *Pramana J. Phys.*, **65**, 801 (2005);
30. M. Jothibas, C. Manoharan, S. Ramalingam, S. Dhanapandian and M. Bououdina, *Spectrochim. Acta A Mol. Biomol. Spectrosc.*, **122**, 171 (2014); https://doi.org/10.1016/j.saa.2013.11.008
31. P. Kumar, N. Saxena, R. Chandra, V. Gupta, A. Agarwal and D. Kanjilal, *Nanoscale Res. Lett.*, **7**, 584 (2012); https://doi.org/10.1186/1556-276X-7-584
32. M. Kashif, M.E. Ali, S.M.U. Ali, U. Hashim and S.B.A. Hamid, *Nanoscale Res. Lett.*, **8**, 68 (2013); https://doi.org/10.1186/1556-276X-8-68
33. V. Singh, P.K. Sharma and P. Chauhan, *Mater. Charact.*, **62**, 43 (2011); https://doi.org/10.1016/j.matchar.2010.10.009
34. A.A. Alghamdi, A.-B. Al-Odayni, W.S. Saeed, M.S. Almutairi, F.A. Alharthi, T. Aouak and A. Al-Kahtani, *Molecules*, **24**, 3685 (2019); https://doi.org/10.3390/molecules24203685
35. V. Ramasamy, V. Mohana and G. Suresh, *Indian J. Phys.*, **92**, 1601 (2018); https://doi.org/10.1007/s12648-018-1246-9